The Influence of Gravity Waves on Radiometric Measurements: A Case Study

M. T. DECKER

Wave Propagation Laboratory, NOAA, Boulder, CO 80303

F. EINAUDI

School of Geophysical Sciences, Georgia Institute of Technology, Atlanta 30332

J. J. FINNIGAN[1]

Cooperative Institute for Research in Environmental Sciences, University of Colorado/NOAA, Boulder, CO 80304

(Manuscript received 6 March 1981, in final form 18 June 1981)

ABSTRACT

During the 1978 PHOENIX experiment at the Boulder Atmospheric Observatory in Colorado, the presence of atmospheric gravity waves was detected by various independent remote sensing instruments. Fluctuations in the zenith atmospheric radiation were measured at 22.235 and 55.45 GHz in the water vapor and oxygen absorption bands and compared with corresponding fluctuations of surface pressure and the height of FM-CW radar echo returns. These fluctuations are explained, qualitatively and quantitatively, in terms of an internal gravity wave generated by wind shear above the boundary layer. The analysis shows that the oscillations at 22.235 GHz are essentially due to fluctuations of water vapor in the antenna beam while those at 55.45 GHz are due to temperature variations.

1. Introduction

Internal gravity waves have been detected in the atmosphere by a variety of passive sensors such as fast response temperature sensors, anemometers and microbarographs or active sensors such as FM-CW radars, acoustic radars, meteor radars and so on. These passive sensors, whether located at the ground or distributed along a meteorological tower or airborne, essentially give the values of the variable they measure at a given position in space and at a given time. The radars measure echoes which are in fact integrated over a height range that depends on the height resolution of the instrument.

More recently, gravity waves have been revealed by ground-based passive devices whose measurements depend on the chemical reactions, temperatures, and number densities of the atmospheric constituents over a finite vertical extent. These measurements must therefore be considered weighted averages over such a height range.

Substantial evidence exists that the rotational temperature of the night-glow emission from OH (at ~90 km height) displays large fluctuations (Krassovsky, 1972; Krassovsky and Shagaev, 1974a,b, 1977; Krassovsky *et al.*, 1975; Noxon, 1978) whose periods, which vary from 20 min to 2 h are well within the range of gravity waves. Indeed, Krassovsky and Shagaev, using three instruments pointing toward the vertices of a base triangle which, at an altitude of 90 km had sides of ~200 km, could also measure the horizontal phase velocity of the disturbance and infer, by ray tracing, that its origin was within the jet stream region in the troposphere below. It is interesting to point out that the same jet stream region was identified as the source of gravity waves revealed by the observations of noctilucent clouds in the mesopause region (Auff'm Ordt and Brodhun, 1974). Armstrong (1975), measuring hydroxyl rotational temperature, also recorded variations that he interprets in terms of a gravity wave: since the wave also was observed by the periodic variations in the height of the F2-layer as shown by a network of ionosondes, Armstrong concludes that it was a gravity wave traveling from high latitudes equatorward, i.e., it was a traveling ionospheric disturbance (TID). Beautiful photographic evidence of wave motions in the OH nightglow has been represented by Moreels and Hersé (1977) and Hersé *et al.* (1980). Noxon has reported the simultaneous measurement of large fluctuations in the atmospheric temperature, using emission from $O_2(^1\Sigma)$ and OH near 95 and 85 km, respectively. The relative amplitudes and phases appear to be consistent with a gravity wave interpretation of the

[1] Permanent affiliation: CSIRO, Division of Environmental Mechanics, P.O. Box 821, Canberra City, A.C.T. 2601, Australia.

0021-8952/81/101231-08$06.00

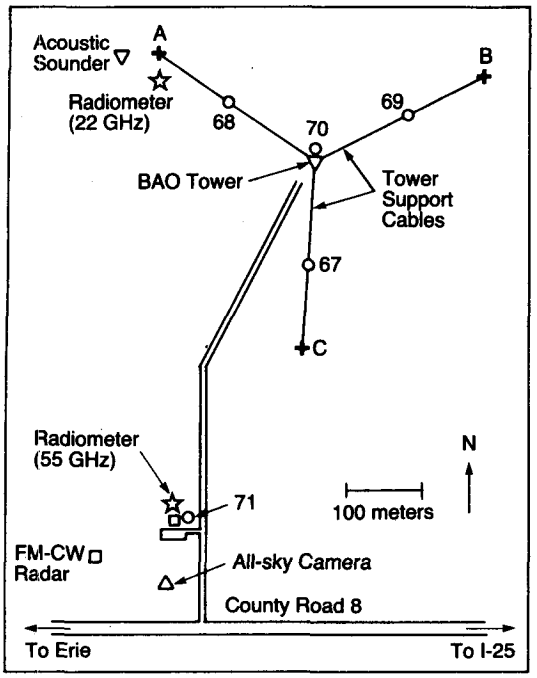

FIG. 1. Map of the operational area around the BAO tower showing microbarographs (0) identified by numbers 67 through 71 and vertices (+) of the optical triangle identified by letters A, B and C.

observation (see, also, Weinstock, 1978). Hernandez and Turtle (1965) report oscillations in the Doppler temperature of the OI (5577 Å) in the nightglow arising near 95 km.

Similar oscillations have been observed in the measurement of thermal radiation from the atmosphere both at microwave and infrared frequencies (Martin and Beard, 1976; Beard and Martin, 1978; Basili and Solimini, 1978; Ciotti *et al.*, 1979). Since radiometric measurements of thermal radiation from the atmosphere have been used to determine the temperature structure in the troposphere (Westwater, 1972; Westwater *et al.*, 1975; Wang *et al.*, 1975; Basili and Solimini, 1978; Decker *et al.*, 1978; and others), it is important to establish how such measurements are affected by the presence of gravity waves.

Gravity waves are motions of the atmosphere in which the various quantities such as pressure, density, velocity and temperature, all vary as a function of time and spatial coordinates in a coherent fashion. The characteristics of the disturbance, horizontal wavelength, period and vertical structure, will be imposed by the mean properties of the atmosphere, i.e., its wind and temperature distributions. In addition, if we think of the atmosphere as a mixture of gases, we recognize that the individual constituents will be affected by the gravity wave in a rather complex way. The number density of each constituent will fluctuate in a manner that also will depend on its background value; if chemical reactions are involved, they will be influenced by the temperature fluctuations because the reaction rates depend on the temperature. The detailed evaluation of how the presence of a gravity wave affects the observed radiometric phenomena is rather complex since it involves calculating the individual parcel displacements as well as integrating appropriate quantities along the beam of the antenna.

With reference to the tropospheric measurements, we can state that the output of the radiometer is essentially the integral along the field-of-view of the antenna beam of the atmospheric Planck function properly weighted by a corresponding radiative transfer kernel (see Ciotti *et al.*, 1979). In the microwave part of the spectrum the Rayleigh-Jeans approximation allows us to write this in terms of a monochromatic brightness temperature T_b as

$$T_b = \int_0^\infty T(r)\alpha(r) \exp\left[-\int_0^r \alpha(r')dr'\right]dr + T_{\text{ext}} \exp\left[-\int_0^\infty \alpha(r)dr\right], \quad (1)$$

where $T(r)$ is the temperature of the atmosphere at distance r from the observation point, $\alpha(r)$ the corresponding absorption coefficient, and T_{ext} the cosmic background radiation external to the atmosphere. It follows that the fluctuating component of the radiometric measurement will depend in general on the periodic variations of both the atmospheric temperature and the partial densities of the atmospheric constituents, the latter dominating the fluctuations in absorption. If the antenna beam is not narrow, integration along the beam is substantially more complex.

We present here a detailed study of the effect of a gravity wave on radiometric measurements carried out at 22.235 and 55.45 GHz, corresponding to the water vapor and the oxygen absorption lines. The wave was observed with various sensors distributed along and around the 300 m tower at the Boulder Atmospheric Observatory near Erie, Colorado. The structure of the wave and of the coexisting turbulence have been analyzed in detail by Einaudi and Finnigan (1981) and Finnigan and Einaudi (1981). They show that a linear model can adequately describe the observed wave. Such a model is used here to reproduce in detail the observations at both frequencies and to show that most of the observed fluctuations at 22.235 GHz are due to water vapor density fluctuations, while those at 55.45 GHz are mainly due to the fluctuations in temperature.

In the next section, we present the experimental configuration, the data and their analysis. In section three, the characteristics of the wave are dis-

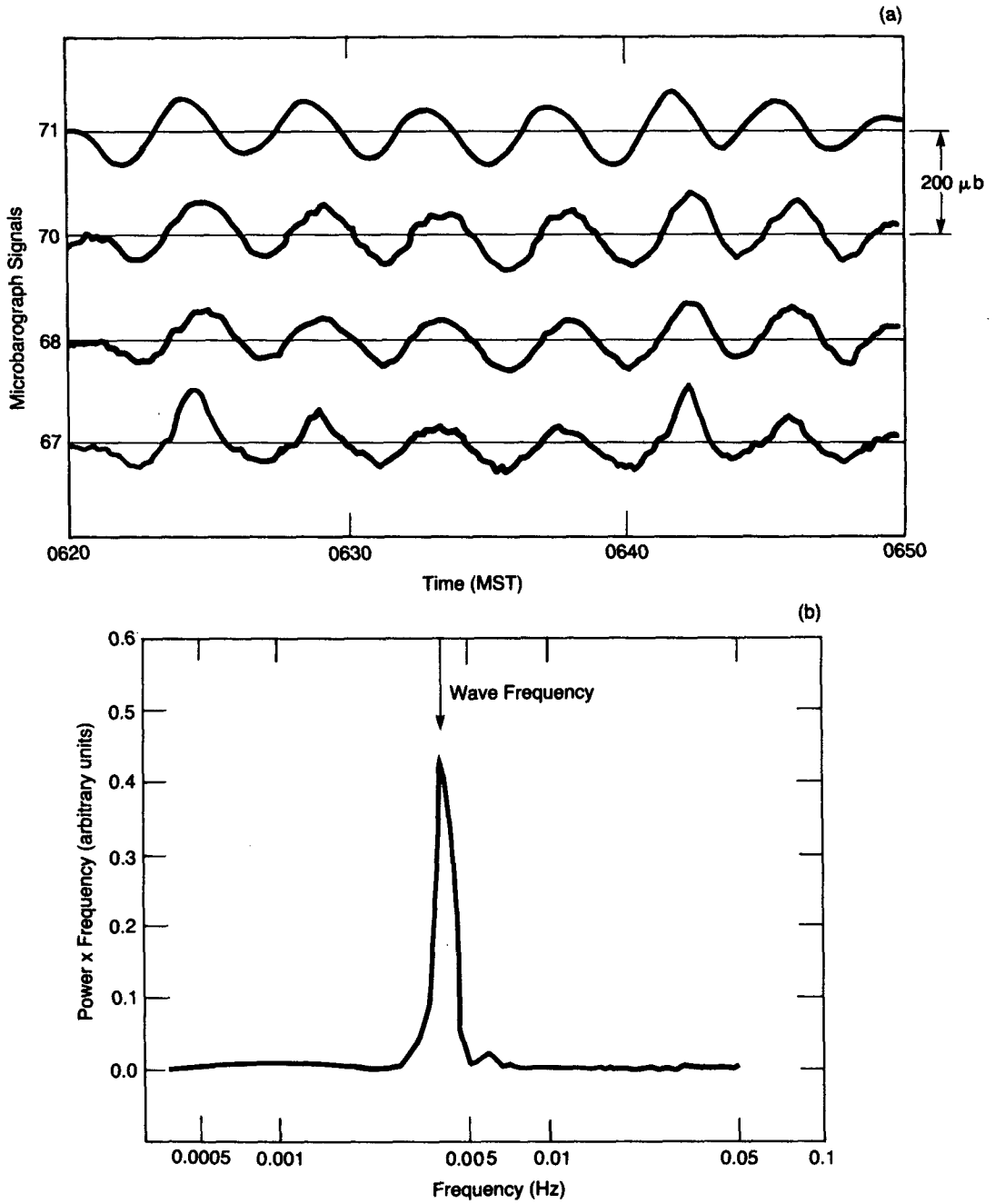

FIG. 2. (a) Traces of the four microbarographs 67, 68, 70 and 71 (see Fig. 1 for their location relative to the tower) as a function of time. (b) Power spectrum of microbarograph 70 at the base of the tower. The spectrum was calculated with 256 points and without smoothing.

cussed and comparisons made with radiometric observations that show the relative effect of temperature and water vapor fluctuations on the brightness measurements.

2. The data and their analysis

The data were obtained at the Boulder Atmospheric Observatory's 300 m tower during the September 1978 PHOENIX boundary-layer experiment (Hooke, 1979). The Observatory is operated by the Wave Propagation Laboratory of the National Oceanic and Atmospheric Administration. During the PHOENIX experiment the anemometers, temperature and vapor sensors permanently located at eight levels along the tower were supplemented by a large variety of sensors. Included were an array

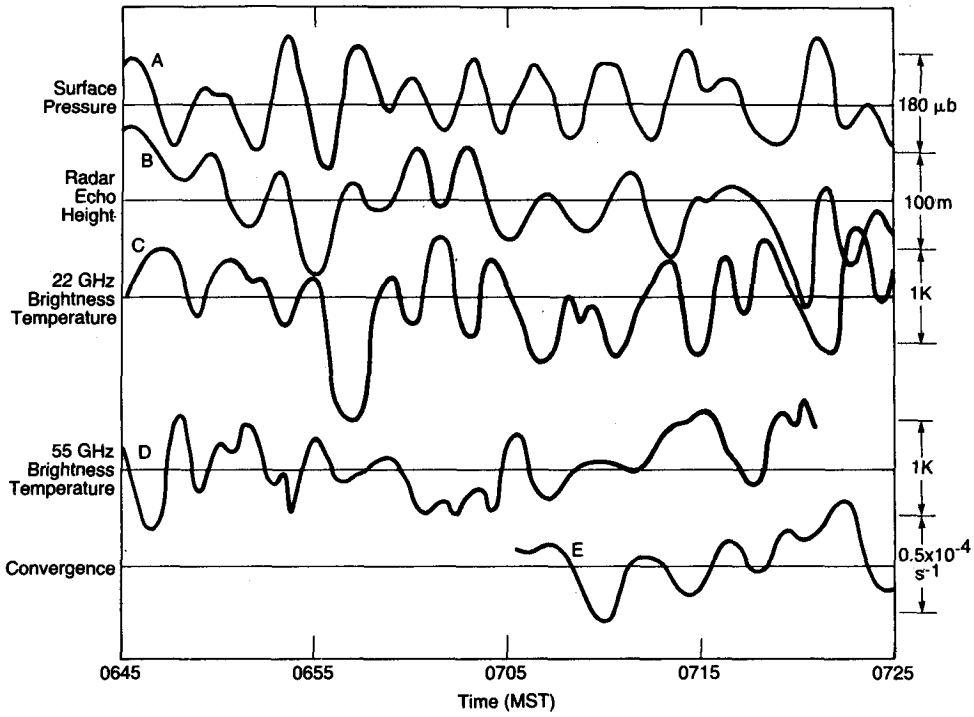

FIG. 3. Traces of surface pressure (curve A); height of maximum echo return (B) as inferred by visual inspection of the FM-CW radar records; brightness temperature at 22.235 GHz (C) and 55.45 GHz (D); and convergence field (E) as a function of time. The time reference for each curve is as recorded by the corresponding sensor (see text).

of Doppler radars, a 10 cm FM-CW radar, an 8 mm cloud study radar, lidar, all-sky camera, an array of acoustic sounders, microwave radiometers, an array of microbarographs, optical measurements of atmospheric convergence, radiosondes, a 27-station network of surface wind/temperature/humidity/rain sensors, and aircraft instrumented for temperature, humidity, winds, pressure, refractive index and cloud particle size. Of particular interest here are the microbarographs, FM-CW radar, microwave radiometers and convergence sensors. The location of these instruments relative to the tower can be seen in Fig. 1.

The best evidence for the presence of the wave comes from the microbarograph records; these were sampled at 0.1 Hz, and their power spectra were calculated using an FFT routine developed by Fraser (1979). The pressure traces from four microbarographs are plotted in Fig. 2a as a function of time starting at 0620 MST 18 September 1978. All four traces reveal a remarkably monochromatic wave with a peak-to-peak amplitude of ~180 μb. The spectral power plot in Fig. 2b for microbarograph 70 (the closest to the tower) confirms the near monochromaticity of the event. The analysis covers about 2 h. Prior to 0620 MST, some of the data were not in usable form although from the FM-CW and acoustic sounder facsimile records it appears that the wave began a few hours earlier. After 0820, the effect of the disturbance is not so clearly detectable because the transition to a convective boundary layer is accelerating.

Time series data from five independent sensors are plotted in Fig. 3. Curve A is a microbarograph record similar to those of Fig. 2 but for the time period 0645 to 0725 MST. It is from sensor 68 near the 22.235 GHz radiometer. It is evident that the trace is less monochromatic than that for the 0620–0650 MST time period of Fig. 2. We use here the 0645–0725 MST time period because radiometric measurements at 22 GHz are not available for earlier times. Curve B represents the variation in height of the return of maximum intensity as inferred by visual inspection of the FM-CW radar records. This radar (Chadwick *et al.*, 1976; Hooke, 1979) was pointed at the zenith during the time period shown, and its spatial resolution is ~6 m. Data were available at a 15 s time interval. The variations in zenith atmospheric radiation (brightness temperature) at 22.235 and 55.45 GHz are plotted in curves C and D, respectively. Finally, the convergence field as inferred from the optical triangle ABC (see Fig. 1) is given by E, starting at about 0700 (see Tsay *et al.*, 1980). The time reference is as recorded for each instrument; specifically the pressure and convergence field data are archived by the BAO data

processing facility with a common time reference, while the FM-CW radar and the radiometric data each has its own time reference; this may result in slight apparent time shifts difficult to estimate. Furthermore, in assessing the phase differences between the various traces we must keep in mind that the instruments are located in different positions as indicated in Fig. 1.

The 22.235 GHz measurements are from an instrument located near the west guy-anchor of the BAO tower as shown in Fig. 1. This radiometer antenna was fixed in the zenith position with data outputs available at 32 s intervals. The 55.45 GHz instrument was located ~600 m south of the 22.235 GHz instrument. In this case, the antenna scanned through zenith angles of ±47° with a dwell time of 1 s at each of 11 positions. Data are available at 15 s intervals, but the higher frequency and short dwell time make these data noisier than those at the lower frequency and so some smoothing of the data was done. The angular width of each antenna beam was ~7°. Measurements were also carried out at other frequencies in the oxygen absorption complex as part of an effort to evaluate the combined use of the radiometers and sensors such as radars, acoustic sounders, and lidars for remotely sensing atmospheric profiles of temperature and humidity.

To complete the data necessary for the analysis, we need the background temperature, humidity and wind. They were obtained from the rawinsonde ascent of 1200 GMT from Denver, Colorado, which is 35 km south of the Erie site. Since the launch time was actually 1100 GMT, the data correspond to a time interval of about 1 h, beginning about 3 h prior to the event we are describing. The rawinsonde data, with the background wind projected into the direction of propagation of the wave, are given in Fig. 4.

3. Interpretation of the results

The spectral analysis and cross correlation of the microbarograph records allow determination of the period τ, the direction α of propagation of the wave, its horizontal phase velocity v_{ph} and, finally, its amplitude at the ground p_0:

$$\left.\begin{aligned} \tau &= (240 \pm 10)\text{s}, & \alpha &= 219.5° \pm 2° \\ v_{ph} &= \omega_r/k = (12.04 \pm 1.2)\text{m s}^{-1}, & p_0 &= (90.3 \pm 9)\mu\text{b} \end{aligned}\right\}, \tag{2}$$

where $\omega_r = 2\pi/\tau$, $k = 2\pi/\lambda$, with λ the horizontal wavelength, equal to (2.8 ± 0.41) km. The derivation of the characteristics of the gravity waves as a linear solution of the equations of motion is given by Einaudi and Finnigan (1981), in which other relevant references are also provided. It suffices to say here that the linear solution is a solution of the linearized equations of motion of the form

$$a(t,x,z) = a(z)\exp[i(\omega t - kx)] + \text{complex conjugate}, \tag{3}$$

where $\omega = \omega_r + \omega_i$, in general, is complex and $a(z)$ is an eigenfunction of a second-order differential equation (the Taylor-Goldstein equation) whose eigenvalues are ω and k. In other words, solutions of the form (3) are modes that the background atmosphere described in Fig. 4 can support.

The calculations show that if we choose to match the value for λ (and therefore for k), the model gives a value for ω such that $v_{ph} = \omega_r/k = 11.51$ m s^{-1} which appears to be close enough to the measured value of 12.04 m s^{-1}. The value for ω_i is 0.8 10^{-4} s^{-1}. To obtain a comprehensive view of the vertical structure of the corresponding eigenfunctions, we reproduce in Fig. 5 the amplitude and phase (with respect to a common arbitrary reference phase) of the vertical displacements and temperature fluctuations as a function of the height. The vertical structure is typical of a Kelvin-Helmholtz wave generated by shear in the neighborhood of 1.1 km, where the Richardson number is in fact less than the critical value of 1/4. The analysis of Einaudi and Finnigan (1981) and Finnigan and Einaudi (1981) confirms that this wave explains adequately not only the observed period τ and wavenumber k, but also the vertical structure of the disturbance as inferred

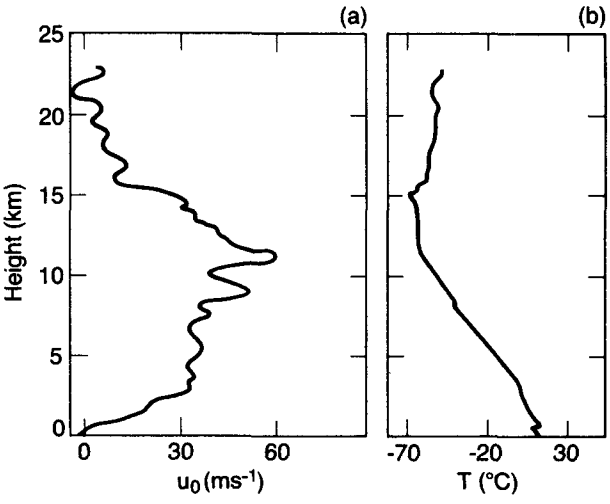

FIG. 4. (a) Profile of the horizontal velocity, projected along the direction of propagation of the wave, obtained from the rawinsonde launch from Denver, at 1200 GMT 18 September 1978. (b) Profile of temperature from same source.

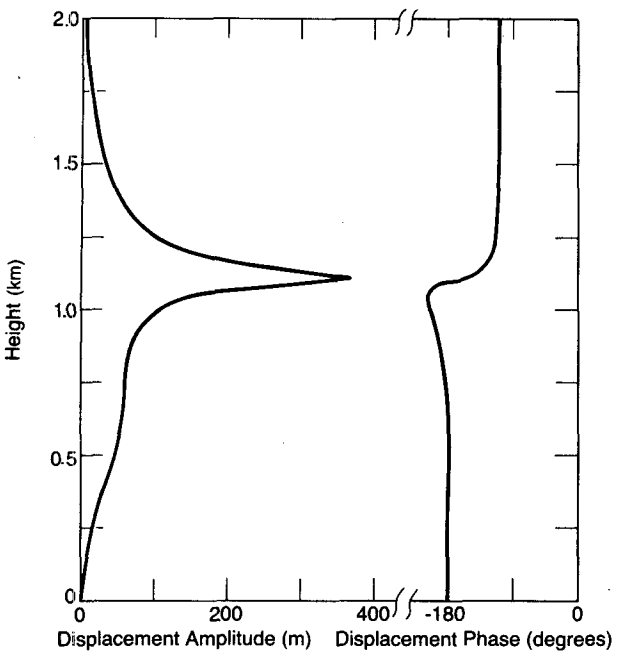

FIG. 5. Profiles of the amplitude and phase of the vertical displacement using the linear model.

from the measurements of temperature and velocity fluctuations along the tower.

A spectral analysis of the radiometric measurements confirms that the fluctuations in brightness temperature at both frequencies have a component with a period on the order of 240 s.

Interesting although somewhat qualitative conclusions about the various processes involved may be immediately inferred from the curves of Fig. 3. Let us first discuss the FM-CW radar echo and the 22.235 GHz brightness temperature, curves B and C. At this frequency the radiometer primarily measures changes in the total integrated water vapor at the zenith and, therefore, one expects a maximum value as the low-level water vapor converges and lifts. The water vapor is all essentially contained below the temperature inversion, which is ~500 m above the surface and whose displacements are revealed by the FM-CW records. If we time shift curve C toward the left by about 45 s to account for the transit time of the wave from the FM-CW radar to the radiometer, then the two records appear to be in phase, within the experimental errors involved in the two reference times mentioned earlier. Radiation at 55.45 GHz is dominated by emission from oxygen. Since variations in the amount of this gas are very small, the variation in observed radiation is the result of temperature changes, especially in the lowest 1 km. The temperature changes result from atmospheric warming and cooling associated with parcel displacements. The model predicts that in this height range temperature and vertical displacements are essentially out of phase. Superposition of the 55.45 GHz and FM-CW traces does indeed show that an out-of-phase component is evident. Somewhat inconclusive is the comparison of traces A and B because there seems to be a sudden time shift of ~90° occurring near the middle of the time interval under consideration. We have no concrete explanation to offer for this time shift. In the first part of the record, however, the vertical displacement of the inversion height resulting from the low-level convergence and lifting associated with the wave, appears to be in phase with the surface pressure. Finally, it should be noted that if we account for the position of the FM-CW radar relative to the midpoint of the ABC triangle, the trace E of the convergence field leads the displacements of the inversion height by about 90°, as expected.

Given the background temperature and humidity profiles from the Denver rawinsonde and the temperature fluctuations and displacements predicted by the wave model, we can compute the changes in radiation to be expected at 22.235 and 55.45 GHz. Fig. 6a shows the temperature changes in the lowest kilometer as the atmosphere is lifted and cooled at the peak of the wave and warmed at the wave trough. Quite large temperature changes occur because of the structure of the elevated temperature inversion near 500 m above the surface. The water vapor profiles of Fig. 6b were constructed by taking the vapor densities of the reference profile and displacing them according to the maximum vertical displacements of the model. Both representations are possible because the phases of the temperature fluctuations and of the vertical displacements are essentially uniform over this height range. In the case of upward displacement, the relative humidity exceeded 100% for a small region and the excess vapor was entered in the profile as cloud liquid, as indicated in the figure. Here we note that the time sequence of all-sky photographs shows a mostly cloudy sky, but with alternating clear and cloudy streaks passing overhead at a speed and direction consistent with the wave model. Although the background profile was measured at Denver, 35 km distant and 3 h earlier than this event, a rawinsonde launch at the BAO site at 0900 MST and temperature data from the tower during the intervening time indicate that the basic profile structure in the lowest kilometer remained relatively constant over this time period.

The examination of these profiles at higher altitudes reveals that the changes there are very small, so we can conclude that the profile changes that cause the fluctuations in microwave radiation occur in the lowest kilometer of the atmosphere. This conclusion is reinforced in the case of 55.45 GHz by the fact that the quantity $\alpha(r)\exp[-\int_0^r \alpha(r')dr']$

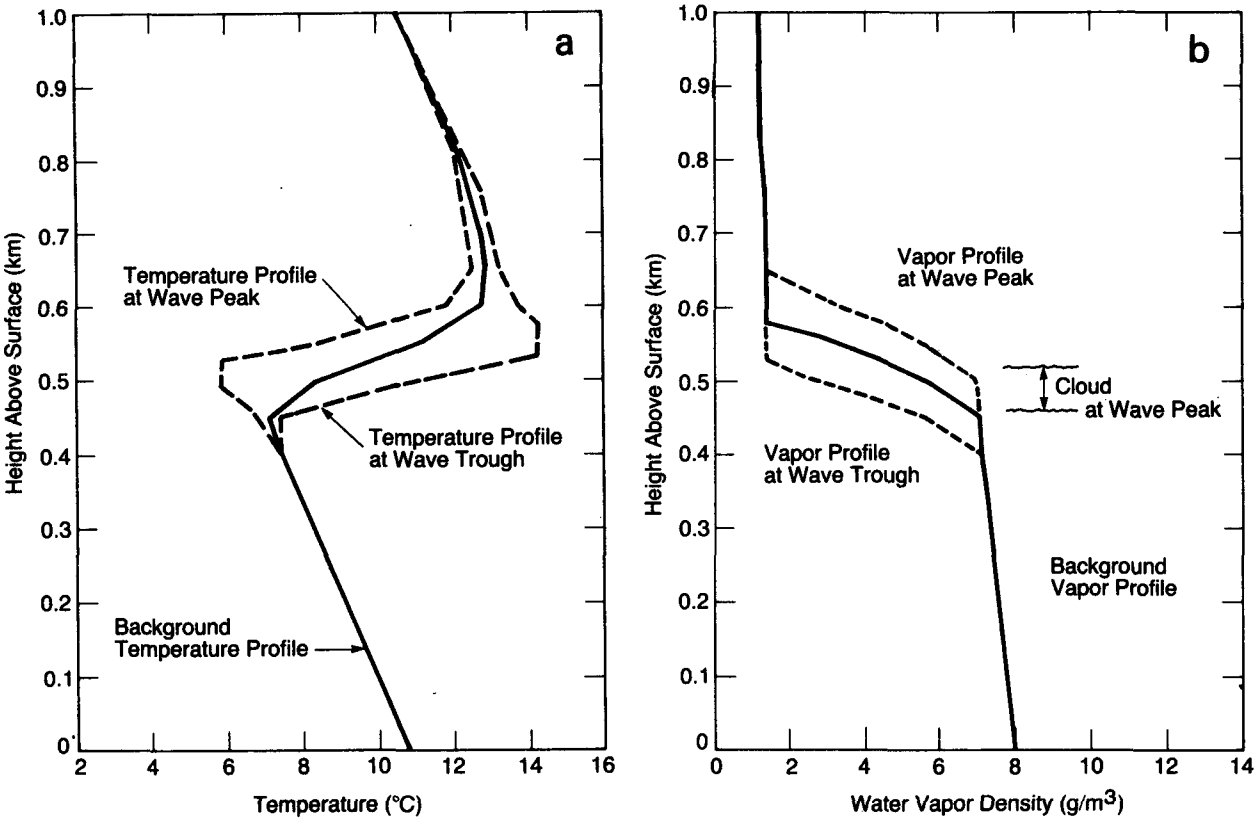

FIG. 6. Temperature (a) and water vapor (b) profiles at wave peak and wave trough. Solid lines are background and dashed lines show maximum variations of the sum of the background plus wave components of the temperature and vapor profiles.

in (1), known as the weighting function, decreases exponentially with height. In this case it is reduced to $1/e$ of the surface value at a height of 880 m. In the case of 22.235 GHz where radiation depends strongly on water vapor, most of the vapor is concentrated below the elevated temperature inversion so that displacements at higher altitudes have a negligible effect.

Finally, the changes in radiation corresponding to the profiles of Fig. 6 have been calculated by solving numerically the equations of radiative transfer. The peak-to-peak changes were 1.26 K at 22.235 GHz and 0.50 K at 55.45 GHz. These values may be compared with the measured fluctuations of Fig. 3. The rms fluctuation of the 22.235 GHz radiation is 0.40 K, which would correspond to a sine wave whose peak-to-peak amplitude is 1.13 K. The rms fluctuation of the 55.45 GHz measurements is 0.31 K, which corresponds to a 0.88 K sine wave. At both frequencies the observed and predicted rms fluctuations are in reasonable agreement, thus increasing our confidence in the ability of the linear model to explain the observations. This point is further confirmed by comparing the displacement amplitude of 92 m predicted by the model at the mean echo height of 485 m, with the equivalent sine wave amplitude of 90.5 m as inferred from curve B of Fig. 3. Since the radar echo height was decreasing during the period of observations, the latter figure was determined by detrending the record with a linear slope such that the rms variations were minimized.

4. Conclusions

We have presented a case study in which the periodic oscillations of measured brightness temperature have been explained in terms of a gravity wave generated by wind shear above the boundary layer. The results provide further evidence that the fluctuations observed in radiometric measurements are due to gravity waves, and they also indicate that linear theory may be adequate to explain the observations.

We have shown that the variations at 55.45 GHz are dominated by temperature fluctuations which tend to be enhanced by temperature inversions, while the oscillations near 22.235 GHz depend on the water vapor integrated along the antenna beam. The latter fluctuations are likely to be present

in any comparable convergence-divergence situations in the presence of water vapor. Indeed, we believe that such observations would be of use in the study of the early development of condensation processes and thus in the analysis of the possible role of gravity waves in lifting water vapor and triggering convective cells.

Finally, it may be appropriate to suggest that care should be exercised in the use of radiometric measurements for inferring background temperature profiles since the measurements may be affected by gravity waves. In particular, it is important that the time over which the measurements are averaged is indeed adequate to filter out the effect of the waves themselves.

Acknowledgments. The authors express their appreciation to the many persons involved in the preparation for and operation of the PHOENIX experiment. Surface pressure measurements were provided by A. J. Bedard, FM-CW radar records by R. B. Chadwick, and convergence data by M.-U. Tsay and T.-I. Wang all of the Wave Propagation Laboratory. Brightness measurements at 22 GHz were made by personnel from the Jet Propulsion Laboratory under the direction of B. L. Gary. C. E. Case of the Wave Propagation Laboratory assisted with the measurements at 55 GHz.

REFERENCES

Armstrong, E. B., 1975: The influence of a gravity wave on the airglow hydroxyl rotational temperature at night. *J. Atmos. Terr. Phys.*, **37**, 1585–1591.

Auff'm Ordt, N., and D. Brodhun, 1974: Zur Deutung von Wellenstrukturen auf Leuchtenden Nachtwolken. *Z. Meteor.*, **24**, 291–294.

Basili, P., and D. Solimini, 1978: Inference of static and dynamic vertical structure of the lower troposphere from ground-based infrared radiometry. *Radio Sci.*, **13**, 303–311.

Beard, C. I., and L. U. Martin, 1978: Microwave radiometric sensing of the marine boundary layer. *Radio Sci.*, **13**, 291–301.

Chadwick, R. B., K. P. Moran, R. G. Strauch, G. E. Morrison and W. C. Campbell, 1976: Microwave radar wind measurements in the clear air. *Radio Sci.*, **11**, 795–802.

Ciotti, P., D. Solimini and P. Basili, 1979: Spectra of atmospheric variables as deduced from ground-based radiometry. *IEEE Trans. Geosci. Electron.*, **GE-17**, 68–77.

Decker, M. T., E. R. Westwater and F. O. Guiraud, 1978: Experimental evaluation of ground-based microwave radiometric sensing of atmospheric temperature and water vapor profiles. *J. Appl. Meteor.*, **6**, 824–836.

Einaudi, F., and J. J. Finnigan, 1981: The interaction between an internal gravity wave and the planetary boundary layer. Part I: The linear analysis. To appear in *Quart. J. Roy. Meteor. Soc.*

Finnigan, J. J., and F. Einaudi, 1981: The interaction between an internal gravity wave and the planetary boundary layer. Part II: Effect of the wave on the turbulence structure. To appear in *Quart. J. Roy. Meteor. Soc.*

Fraser, D., 1979: An optimized mass storage FFT. *Programs for Digital Signal Processing*, Digital Signal Processing Committee, ASSP Society, IEEE Press, 445 Hoes Lane, Piscataway, NJ 08854.

Hernandez, G. J., and J. P. Turtle, 1965: Nightglow 5577 Å (OI) line kinetic temperatures. *Planet. Space Sci.*, **13**, 901–904.

Hersé, M., G. Moreels and J. Clairemidi, 1980: Waves in the OH emissive layer: photography and topography. *Appl. Opt.*, **19**, 355–362.

Hooke, W. H., Ed., 1979: Project PHOENIX, The September 1978 Field Operation. Joint publication of NOAA/ERL and NCAR. [U.S. Govt. Printing Office, SD No. 003-017-00474-1].

Krassovsky, V. I., 1972: Infrasonic variations of OH emission in the upper atmosphere. *Ann. Geophys.*, **28**, 739–746.

——, and M. V. Shagaev, 1974a: Optical method of recording acoustic or gravity waves in the upper atmosphere. *J. Atmos. Terr. Phys.*, **36**, 373–375.

——, and ——, 1974b: Inhomogeneities and wavelike variations of the rotational temperature of atmospheric hydroxyl. *Planet. Space Sci.*, **22**, 1334–1337.

——, and ——, 1977: On the nature of internal gravitational waves observed from hydroxyl emission. *Planet. Space Sci.*, **25**, 200–201.

——, K. I. Kuzmin, N. A. Piterskaya, A. I. Semenov, M. V. Shagaev, N. N. Shefov and T. I. Toroshelidze, 1975: Results of some airglow observations of internal gravitational waves. *Planet. Space Sci.*, **23**, 896–898.

Martin, L. U., and C. I. Beard, 1976: Microwave radiometric detection of atmospheric internal waves. *Geophys. Res. Lett.*, **3**, 327–330.

Moreels, G., and M. Hersé, 1977: Photographic evidence of waves around the 85 km level. *Planet. Space Sci.*, **25**, 265–273.

Noxon, J. F., 1978: Effect of internal gravity waves upon night airglow temperatures. *Geophys. Res. Lett.*, **5**, 25–27.

Tsay, M.-K., T.-I. Wang, R. S. Lawrence, G. R. Ochs and R. B. Fritz, 1980: Wind velocity and convergence measurements at the Boulder Atmospheric Observatory using path-averaged optical wind sensors. *J. Appl. Meteor.*, **19**, 826–833.

Wang, J. Y., C. R. Claysmith and M. Griggs, 1975: Measurement of lower atmospheric temperature profiles from ground-based infrared observations. *J. Appl. Meteor.*, **14**, 308–318.

Weinstock, J., 1978: Theory of the interaction of gravity waves with $O_2(^1\Sigma)$ airglow. *J. Geophys. Res.*, **83**, 5175–5185.

Westwater, E. R., 1972: Ground-based determination of low altitude temperature profiles by microwaves. *Mon. Wea. Rev.*, **100**, 15–28.

——, J. B. Snider and A. V. Carlson, 1975: Experimental determination of temperature profiles by ground-based microwave radiometry. *J. Appl. Meteor.*, **14**, 524–539.